

# Optimized Design of W-Band Quasi-Optical Lens by Using Optical Simulator and Numerical Analysis

Qike Chen<sup>\*</sup>, Yong Fan, and Kaijun Song

**Abstract**—A large aperture quasi-optical dielectric lens antenna for passive imaging at W-band frequency is proposed. The lens is designed to obtain best resolution at a designate distance of 3.5 m from it. The lens has biconvex aspheric surface to achieve low aberration. The initial parameters of the optical path are obtained with Gaussian beam method, and then the optical simulator ZEMAX is applied to optimize the shape of the lens which improves design efficiency greatly. A hybrid numerical method is used to analyze near field distribution of the lens, and the final design of the lens is evaluated and determined by the results. The method is the combining of ANSOFT HFSS software, ray tracing method and integration algorithm based on Huygens' Principle. It is feasible and efficient for the analysis of various lens antennas, such as large aperture lens antennas which are difficult to be simulated by commercial electromagnetic simulation software. The lens is fabricated with HDPE. Experimental results show that its 3 dB beam size is 29 mm at distance of 3.5 m, which is in good agreement with theoretical calculation. The measured patterns on the image plane show that the lens has 0.3 dB decrease of field intensity in field view of 690 mm. Imaging result shows that the lens is a good candidate for focal plane imaging.

## 1. INTRODUCTION

Millimeter wave (MMW) can pass through non-metallic materials such as plastics or cloths with little losses and be nearly totally reflected by metallic materials. This makes MMW technology favorable for security surveillance, especially for the detection of weapons concealed under peoples' clothes [1–4]. Focal plane array (FPA) technology is useful for MMW imaging system due to its ability of greatly increasing the imaging frame rate [5].

For security surveillance, the suitable distance between target and security device is  $2 \sim 4$  m. Image quality will decrease because of degradation of resolution and diffusive attenuation at such a distance for a MMW imaging system. A quasi-optical lens antenna is often used to improve these problems. The critical parameters for MMW imaging system include spatial resolution (SR), field of view (FOV) and depth of field (DOF), and all these parameters are determined by the performance of lens mostly [6]. For example, the SR depends on the beam waist radius of the lens, and the FOV is decided by the beam scanning ability of the lens. The object and image distance of lens are important issues for imaging system designed for security check too.

Previous works have demonstrated various design methods of quasi-optical lens [7–10]. Most of the lenses were designed on the basis of equivalent optical path condition and optimized by ray-tracing method. Such a method is quite suitable for lens which collimates wave into plane wave in its far-zone. However, for a quasi-optical lens which converges the incident divergent spherical wave to a point in its near zone, the method will not provide accurate results of some important parameters, such as the location and radius of beam waist of the lens, due to the effect of diffraction.

---

*Received 8 January 2016, Accepted 23 February 2016, Scheduled 8 March 2016*

<sup>\*</sup> Corresponding author: Qike Chen (qkchen@uestc.edu.cn).

The authors are with the University of Electronic Science and Technology of China, China.



according to Gaussian beam transformation formula:

$$S_2 = f + \frac{S_1 - f}{(S_1/f - 1)^2 + z_c^2/f^2} \quad (2)$$

The parameters of the optical path are listed in Table 1.

**Table 1.** Summary of optical path parameters of the lens.

Parameters	Diameters	$S_o$	$S_i$	$f$	Magnification ( $S_i/S_o$ )
Values	430 mm	3500 mm	712 mm	592 mm	0.203

### 3. QUASI-OPTICS DESIGN AND ANALYSIS

The quasi-optics configuration of the lens and feed antenna is shown in Fig. 2. The quasi-optical lens is designed with biconvex aspheric surface. Such a lens has advantage of lower aberration blurring than spherical biconvex lens and plano-convex lens. The design formula of the aspheric surface is based on the conic equation which is shown as follow:

$$z = \frac{t^2}{R + \sqrt{R^2 - (1+k)t^2}} + at^2 + bt^4 + ct^6 + dt^8 + et^{10} \quad (3)$$

where  $t$  and  $z$  are the coordinates of the lens contours;  $R$  is the curvature radius of the aspheric surface;  $k$  is the conic constant;  $a$ ,  $b$ ,  $c$ ,  $d$  and  $e$  are the high-order coefficients of the conic equation.

The values of the coefficients in Equation (3) are optimized to achieve low aberration by optical simulator ZEMAX. It is very convenient and efficient to design MMW quasi-optical lens by using ZEMAX. However, since ZEMAX is an optical simulator designed for lights illumination system, further simulation needs to be processed to verify the design result when it is used to design MMW lens. Near field of the lens is calculated with the numeric method described in the next section, and the radius and location of the beam waist in object space are obtained to evaluate the design. Numeric result shows that the calculated  $S_o$  will be smaller than the design value in ZEMAX. For example, for lens optimized by ZEMAX with  $S_o = 3500$  mm, the calculated  $S_o$  is only 3184 mm.

The final values of the constants in Equation (3) for both surfaces are given in Table 2. The diameter of the lens is 430 mm, corresponding to  $128\lambda$  at central frequency 89 GHz. Material of the lens is HDPE (high density polyethylene), which has refractive index of 1.508 and loss tangent of  $9 \times 10^{-4}$ . Numeric analysis shows that  $S_o$  of the lens is 3506 mm when  $S_i = 712$  mm.

As discussed in Section 1, the aperture size of the feed horn is limited to 6.1 mm. A horn with aperture size of 8.06 mm  $\times$  5.8 mm and depth of 10.4 mm was simulated and then fabricated. The horn

**Table 2.** Final values of the constants in Equation (3) for both surfaces of lens.

Constant	Left	Right
$R$	12583.41	277.78
$k$	2726.94	$-1.22e - 2$
$a$	$1.17e - 3$	$-2.16e - 3$
$b$	$3.66e - 10$	$-4.82e - 9$
$c$	$-2.04e - 14$	$-6.10e - 14$
$d$	$9.26e - 19$	$8.61e - 19$
$e$	$-1.37e - 23$	$-2.16e - 23$

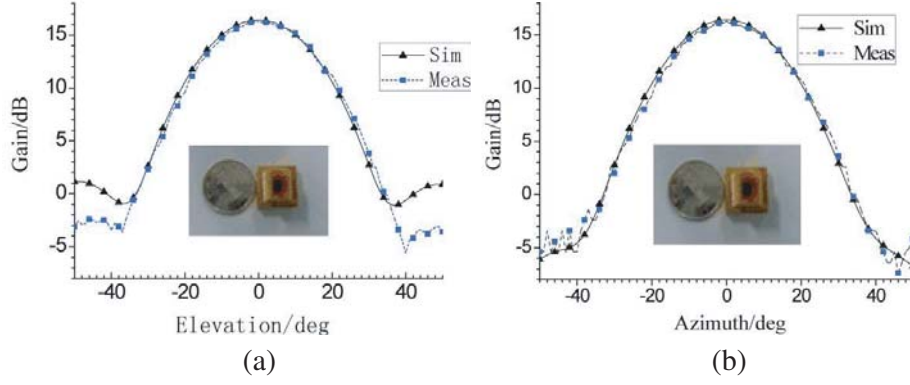


**Figure 3.** The simulated and measured pattern of the feed horn. (a) *E*-plane. (b) *H*-plane.

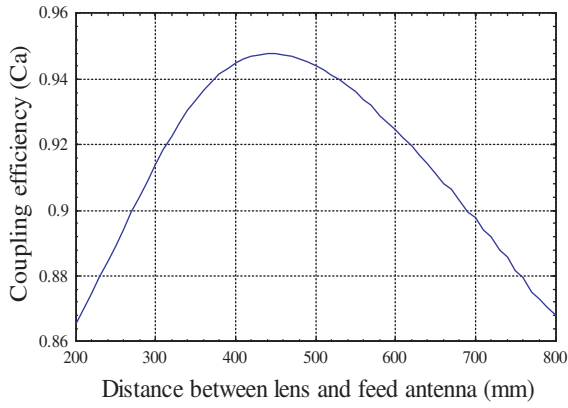


**Figure 4.** Field coupling efficiency  $c_a$  versus distance between lens and feed horn.

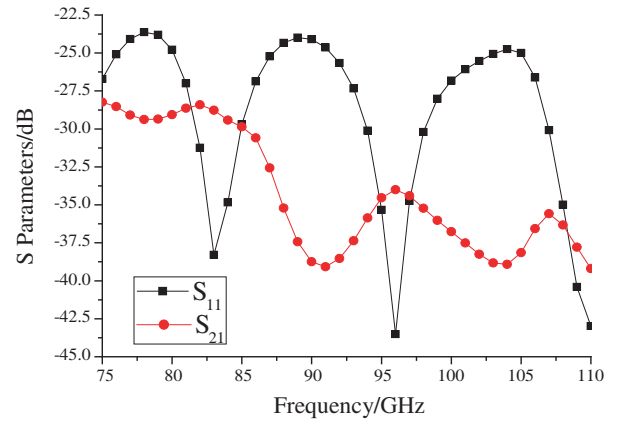


**Figure 5.** Simulation results of coupling between horns.

has gain about 16.2 dB, and its 10 dB beam-width at *E*-plane is  $50^\circ$  and  $52^\circ$  at *H*-plane. The simulated and measured *E* and *H*-field radiation patterns at 89 GHz frequency are depicted in Fig. 3.

The coupling efficiency between the feed horn and lens is evaluated here. The field intensity distribution of a lens is usually treated as Gaussian beam which is expressed as  $q(r) \propto e^{-[r/\omega]^2}$ . The transformation efficiency between Gaussian beam and the radiation pattern of the feed horn  $f(\varphi)$  is depicted as follow [12]:

$$c_a = \frac{\int_{-\psi_m}^{\psi_m} q(r)f(\varphi)d\varphi}{\left[ \int_{-\psi_m}^{\psi_m} |q(r)|^2 d\varphi \int_{-\pi/2}^{\pi/2} |f(\varphi)|^2 d\varphi \right]^{\frac{1}{2}}} \quad (4)$$

Since the Gaussian beam  $q(r)$  is truncated at the edge of the projected aperture of the lens, the integral extends over the range which is determined by the aperture of the lens. As we can see in Fig. 2,  $\psi_m = \tan^{-1}(d/2D)$ , where  $d$  denotes the distance between the lens and the feed horn, which means that  $c_a$  is a function of  $d$ .

The values of  $c_a$  at various  $d$  are calculated by MATLAB and depicted in Fig. 4.  $f(\varphi)$  is the *E*-pattern of the feed which is shown in Fig. 3. The maximum value 0.947 occurs when  $d$  equals 450 mm. When the value of  $d$  increases to 712 mm,  $c_a$  falls to 0.896. It shall be noted that the spillover loss has been included in formula (4).

The feed linear array of the lens consists of 24 horns which are closely packed on its image plane.

The mutual coupling between adjacent elements is analyzed by simulating the  $S$  parameters using ANSYS HFSS. The spacing between the horns is 6.1 mm. The simulation result is shown in Fig. 5. As we can see,  $S_{21}$  is less than  $-28$  dB within the frequency band from 75 GHz to 110 GHz.

#### 4. NUMERICAL ANALYSIS OF QUASI-OPTICS

To obtain the output near field of the lens, the quasi-optical configuration is divided into three parts, and three numerical methods are used to simulate the propagation of  $E$ -field within different regions, as shown in Fig. 2.

The radiation field of the feed horn is calculated with aperture field integration method. The horn aperture is meshed and split into  $N$  triangular elements by using ANSYS software first, and each triangular element has three nodes:  $P_{i1}(x_{i1}, y_{i1}, z_{i1})$ ,  $P_{i2}(x_{i2}, y_{i2}, z_{i2})$ ,  $P_{i3}(x_{i3}, y_{i3}, z_{i3})$ , as shown in Fig. 6. Then the  $E$  and  $H$  fields at all of the grid nodes are calculated with field calculator of HFSS. HFSS is a popular commercial simulator which can solve complicated electromagnetic problem with high accuracy. Then the far field of  $i$ -th triangular element can be given by [13]

$$\bar{E}_{pi} = \bar{e}_\theta E_{\theta i} + \bar{e}_\varphi E_{\varphi i} \quad (5)$$

$$\begin{aligned} E_{\theta i} &= \frac{jk}{4\pi} \frac{e^{-jkR}}{R} \left[ (E_{ix} \cos \varphi + E_{iy} \sin \varphi) + \sqrt{\frac{\mu_0}{\varepsilon_0}} \cos \theta (H_{iy} \cos \varphi - H_{ix} \sin \varphi) \right] e^{jk \sin \theta (x_i \cos \varphi + y_i \sin \varphi)} S_i \\ E_{\varphi} &= \frac{jk}{4\pi} \frac{e^{-jkR}}{R} \left[ \cos \theta (E_{iy} \cos \varphi - E_{ix} \sin \varphi) - \sqrt{\frac{\mu_0}{\varepsilon_0}} (H_{ix} \cos \varphi + H_{iy} \sin \varphi) \right] e^{jk \sin \theta (x_i \cos \varphi + y_i \sin \varphi)} S_i \end{aligned} \quad (6)$$

where  $x_i$  and  $y_i$  are the coordinates of the central point  $P_i$  of  $i$ -th element;  $S_i$  denotes the area of  $i$ -th element;  $R, \theta, \varphi$  are the spherical coordinates of field point;  $E_{ix}$ ,  $E_{iy}$ ,  $H_{ix}$ ,  $H_{iy}$  are the  $E$  and  $H$  field components at  $P_i$ , which can be approximated by

$$\begin{aligned} E_{ix} &= (E_{ix1} + E_{ix2} + E_{ix3})/3, & E_{iy} &= (E_{iy1} + E_{iy2} + E_{iy3})/3 \\ H_{ix} &= (H_{ix1} + H_{ix2} + H_{ix3})/3, & H_{iy} &= (H_{iy1} + H_{iy2} + H_{iy3})/3 \end{aligned} \quad (7)$$

By summarizing the radiation fields of all the triangular elements, the far field of the horn is obtained.

Next, ray-tracing method is processed to simulate the electromagnetic field propagating in the lens. Normally, ray-tracing method includes two steps: (1) obtaining all the ray paths based on Snell's law; (2) calculating electric fields of all rays. Considering that the circular aperture plane is the projection plane of the curved surface of the lens, we split the aperture plane into triangular elements by using ANSYS first, and the  $x$ ,  $y$  coordinates of each node are given by the software. Then the value of  $z$  coordinate of each node is calculated by substituting  $t = \sqrt{x^2 + y^2}$  into formula (3). Thus the curved surface at illumination side of the lens is split into triangular elements, and each node corresponds to one ray.

For single lens condition, each ray path contains two nodes located on the two surfaces of the lens. The first node  $P_1$  is meshing grid node, and the second node  $P_2$  is the intersection point of the refracted

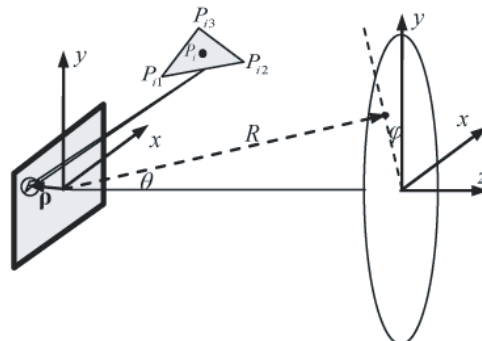


**Figure 6.** Geometry of the triangulation of the feed horn aperture.

ray and second surface of the lens. The coordinates of  $P_2$  can be calculated based on Snell's law. After the ray-tracing process is completed, the second surface of the lens is split into triangular elements by the ray paths, and  $P_2$  is taken as the grid node.

The electric fields at  $P_2$  is calculated with method based on Fresnel's law and the law of power conservation. The incident field  $\bar{E}_1^i$  at  $P_1$  is the radiation field of the feed which is obtained with the method mentioned above. Then the incident field at  $P_2$  is given by

$$\bar{E}_2^i = (\bar{E}_{1v}^i T_{1v} + \bar{E}_{1p}^i T_{1p}) \cdot DF_1 \cdot L_{\varepsilon_r} \cdot e^{-jkR_{12}} \quad (8)$$

where  $\bar{E}_{1v}^i$  and  $\bar{E}_{1p}^i$  are the components of  $\bar{E}_1^i$  which are perpendicular and parallel to the incident plane respectively;  $T_{1v}$  and  $T_{1p}$  are the Fresnel transmission coefficients at  $P_1$ ;  $R_{12}$  is the distance between  $P_1$  and  $P_2$ ;  $L_{\varepsilon_r}$  is the dielectric loss of the lens, which can be obtained as follow [14]

$$L_{\varepsilon_r} = 10^{-\left(\frac{27.3 \cdot R_{12}}{20\lambda} \cdot \tan \delta \cdot \frac{n}{n-1}\right)} \quad (9)$$

in which  $n$  is the index of refraction,  $\tan \delta$  the loss tangent of the medium, and  $\lambda$  the wave length.  $DF_1$  is the divergence factor of the ray and expressed as

$$DF_1 = \frac{1}{\sqrt{1 + R_{12}/\rho_{11}} \sqrt{1 + R_{12}/\rho_{12}}} \quad (10)$$

where  $(\rho_{11}, \rho_{12})$  are the two principal radii of curvature of the transmitted wave front passing through point  $P_1$ , and they can be calculated by the method given by Lee et al. [15]. Finally, the refracted field  $\bar{E}_2^t$  can be yielded by multiplying the transmission coefficient at  $P_2$ .

Now the seconde surface of lens is subdivided into triangular elements by the ray paths, and the field  $\bar{E}_2^t$  at all the nodes is obtained. Then the output fields of lens can be calculated by the method based on Huygens' Principle, which is known as Stratton-Chu formula:

$$\bar{E}_p = -\frac{j}{4\pi\omega\varepsilon} \int_s [k^2 \bar{J}_e + (\bar{J}_e \cdot \nabla) \nabla - j\omega\varepsilon \bar{J}_m \times \nabla] \frac{\exp(-jkr_s)}{r_s} ds \quad (11)$$

Formula (11) can be expressed as follow:

$$\bar{E}_p = \bar{E}_1 + \bar{E}_2 + \bar{E}_3 \quad (12)$$

in which

$$\begin{aligned} \bar{E}_1 &= -\frac{jk^2}{4\pi\omega\varepsilon} \sum_{i=1}^N \left[ -(\bar{J}_{ei} \cdot \bar{r}_{si}) \bar{r}_{si} + \bar{J}_{ei} + \sqrt{\frac{\varepsilon}{\mu}} \bar{J}_{mi} \times \bar{r}_{si} \right] \frac{\exp(-jkr_{si})}{r_{si}} \Delta s_i \\ \bar{E}_2 &= -\frac{j^2 k}{4\pi\omega\varepsilon} \sum_{i=1}^N \left[ 3(\bar{J}_{ei} \cdot \bar{r}_{si}) \bar{r}_{si} - \bar{J}_{ei} - \sqrt{\frac{\varepsilon}{\mu}} \bar{J}_{mi} \times \bar{r}_{si} \right] \frac{\exp(-jkr_{si})}{r_{si}^2} \Delta s_i \\ \bar{E}_3 &= -\frac{j}{4\pi\omega\varepsilon} \sum_{i=1}^N [3(\bar{J}_{ei} \cdot \bar{r}_{si}) \bar{r}_{si} - \bar{J}_{ei}] \frac{\exp(-jkr_{si})}{r_{si}^3} \Delta s_i \end{aligned} \quad (13)$$

where  $N$  is the number of the grid elements;  $\bar{r}_{si}$  is the unit vector in the direction from  $i$ -th element to field point;  $\Delta s_i$  is the area of the  $i$ -th triangular element;  $\bar{J}_{ei}$  and  $\bar{J}_{mi}$  are the equivalent current and magnetic current at  $i$ -th triangular element, which are

$$\bar{J}_{ei} = \bar{n}_i \times \bar{H}_{si}, \quad \bar{J}_{mi} = -\bar{n}_i \times \bar{E}_{si} \quad (14)$$

in which  $\bar{n}_i$  is the unit normal vector of  $i$ -th triangle, and  $\bar{E}_{si}$  and  $\bar{H}_{si}$  are the average fields of the three nodes of  $i$ -th triangular element.

The electric field distribution on the optical axis and the beam pattern at the waist of the lens were calculated with the hybrid numerical method. To evaluate the effectiveness of the method, we simulated the near field of the lens using FEKO 5.5, and then both of the results were compared with the measurement results. The results of electric field distribution on the optical axis are shown in Fig. 7. It can be seen that the numerical results are closer to the measurement results than FEKO's. The maximum power occurs at 3460 mm in numerical method, which is close to the measured value of

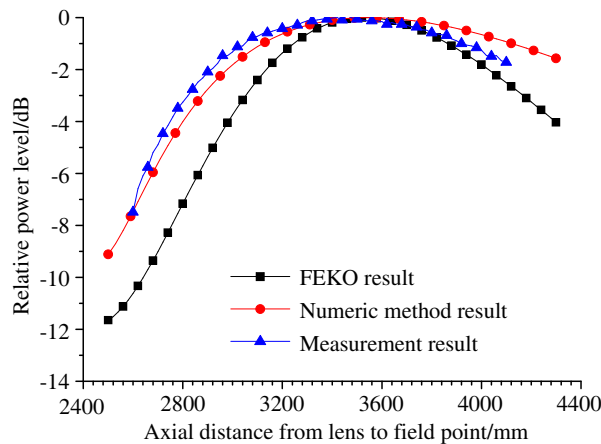


**Figure 7.** Numerical and measurement result of electric field distribution along optical axis comparing with FEKO simulation result.

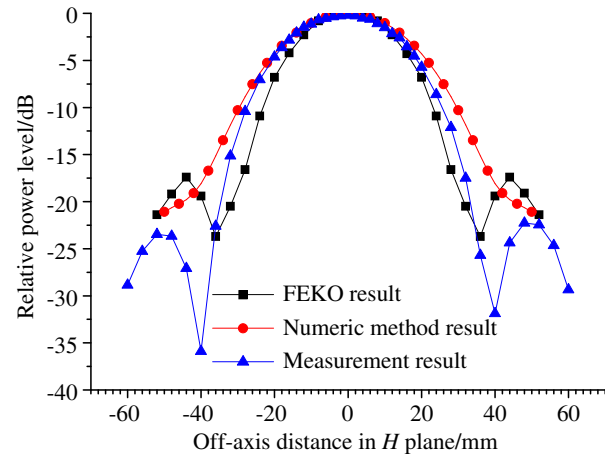


**Figure 8.** Theoretical and measurement result of  $H$ -plane pattern at the beam waist of the lens.

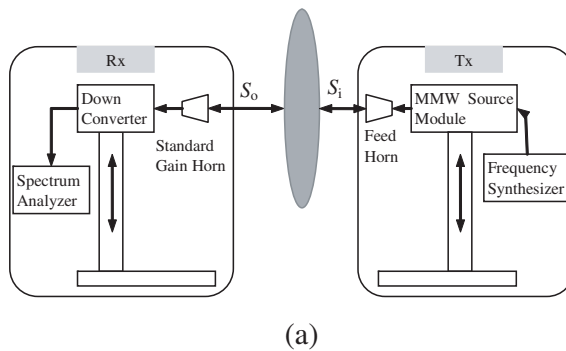


**Figure 9.** (a) Block diagram and (b) photograph of the measurement setup.

3420 mm. The  $H$ -plane pattern at beam waist of the lens is also calculated with numeric method and FEKO, and the results are shown in Fig. 8. The HPBW of the pattern of the numeric result is about 33 mm, which is slightly broader than the measurement result of 29.5 mm.

The hybrid numerical method is very flexible and suitable for analyzing various lenses. Moreover, the method has an advantage in computational time. For the lens proposed in this paper, it takes only about 2.5 seconds to calculate the field at one field point, versus 13 seconds with the FEKO software on the same computer which has processor of core i5 with a CPU frequency of 2.6 GHz and 4 GB of RAM.

## 5. EXPERIMENT RESULT

The quasi-optical lens antenna was fabricated and measured. The quasi-optics experiment setup is shown in Fig. 9. The transmitter was composed of a feed horn and a W-band source generator. A standard gain horn connected with a harmonic down-conversion mixer was applied as receiver, and a spectrum analyzer was used to measure and display the received power. The receiver was placed in object space, and the transmitter was placed in image space. To measure the near-field pattern of the lens, both the transmitter and receiver were fixed on mechanisms which could move in  $x$ ,  $y$ ,  $z$  directions.

The focal length  $f$  was tested first. The distance between the receiver and the lens was fixed at 3500 mm, and then the transmitter was scanned on the optical axis of lens. The focal point was obtained when the maximum power was observed. As we can see in Fig. 10, the maximum power occurs at  $S_i = 682$  mm. According to the thin lens equation, the actual value of focal length  $f$  of the lens is

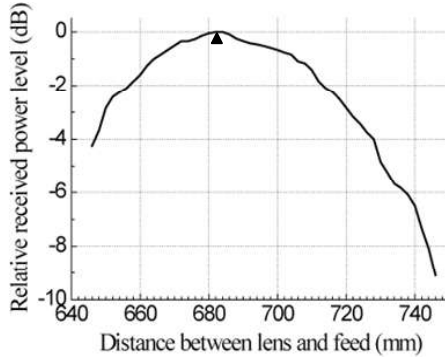


**Figure 10.** Relative received power at various image distance ( $S_o = 3500$  mm).

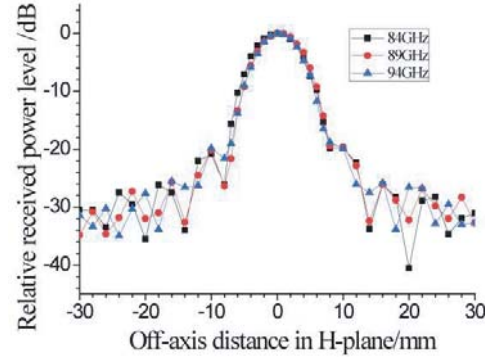


**Figure 11.**  $H$ -plane beam pattern of the lens at various frequency ( $S_i = 682$  mm,  $S_o = 3500$  mm).

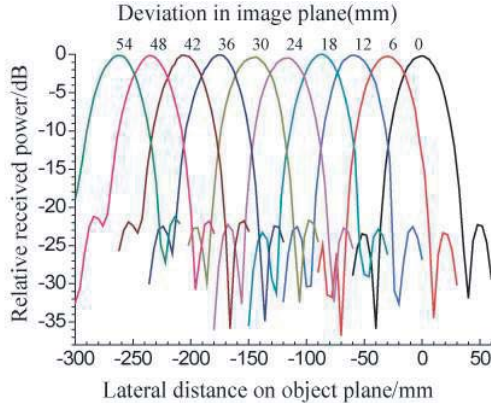


**Figure 12.** Measured beam patterns on the object plane.

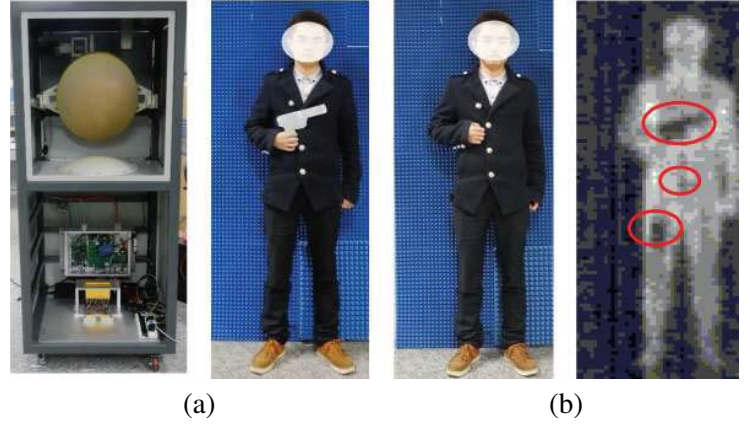


**Figure 13.** (a) Photos of the PMMW imaging system and (b) the imaging result of concealed objects under clothes.

about 571 mm, which is 21 mm smaller than the theoretical value. The difference between the measured value and theoretical value of focal length can be caused by the difference between actual and theoretical value of the dielectric constant of HDPE at W-band.

Then the transmitter and receiver were positioned at  $S_i = 682$  mm and  $S_o = 3500$  mm, respectively. The beam patterns in the image plane at 84, 89, 94 GHz frequency were measured by scanning the transmitter laterally. Measurement results show that the beam patterns are similar for all frequencies, and the 3 dB beam size in the image plane is about 6.4 mm (as seen in Fig. 11).

Further, the measurement of the beam patterns for different lateral deviations were performed. Fig. 12 shows the measured beam patterns on the object plane. The patterns correspond to the situation that the transmitter deviates the optical axis laterally 0 mm, 6 mm, 12 mm, ..., 54 mm in the image plane respectively. As we can see, the HPBW of the beam spot is about 29 mm, and the power intensity fluctuation is less than 0.3 dB.

The quasi-optical lens was applied to the PMMW imaging system. The optical subsystem of the imaging system was composed of the dielectric lens, a 24-channel sensor array and a flapping reflector, as shown in Fig. 13. The imaging sensor array was arranged in a line and located at focal plane of the lens to obtain a field of view of 690 mm  $\times$  1800 mm. The speed of the flapping reflector was regulated so as to realize a frame rate of 4 Hz. Imaging of concealed objects in clothes was performed in the laboratory. A thin metal in the shape of pistol was concealed under clothes of the experimenter, and a hand phone was put in his right trouser pocket. As we can see in Fig. 13, clear images of both targets are obtained in the original MMW image, and the shapes of the targets are shown correctly. Moreover, the image of belt buckle is also displayed.

## 6. CONCLUSION

A large aperture quasi-optical lens antenna used for W-band focal plane millimeter wave imaging has been developed. The shape of the lens was optimized with commercial optical simulator ZEMAX. A flexible and efficient hybrid numerical method was introduced to optimize the design so as to obtain best spatial resolution at designate object distance. Prototype of the lens was fabricated and measured. The lens has an effective focal length of 571 mm and 3 dB beam size about 30 mm on object plane. Experimental results agrees with the numerical calculation quite well.

## REFERENCES

1. Yujiri, L., M. Shoucri, and P. Moffa, "Passive millimeter wave imaging," *IEEE Microwave Magazine*, Vol. 4, No. 3, 39–50, 2003.
2. Stanko, S., D. Notel, A. Wahlen, et al., "Active and passive mm-wave imaging for concealed weapon detection and surveillance," *The 33rd International Conference on Infrared, Millimeter and Terahertz Waves*, 1–2, 2008.
3. Pati, P. and P. Mather, "Open area concealed weapon detection system," *Proceeding of SPIE 8017, Detection and Sensing of Mines, Explosive Objects, and Obscured Targets XVI*, 801702-1–801702-9, Orlando, 2011.
4. Shi, X. and M. H. Yang, "Development of passive millimeter wave imaging for concealed weapon detection indoors," *Microwave and Optical Technology Letters*, Vol. 56, No. 7, 1701–1706, 2014.
5. Sato, S., K. Sawaya, K. Mizuno, et al., "Passive millimeter-wave imaging for security and safety applications," *Proceedings of SPIE 7671, Terahertz Physics, Devices, and Systems*, 76710V-1–76710V-11, 2010.
6. Kim, W. G., N. W. Moon, M. K. Singh, et al., "Characteristic analysis of aspheric quasi optical lens antenna in millimeter-wave radiometer imaging system," *Applied Optics*, Vol. 52, No. 6, 1122–1131, 2013.
7. Thakur, J. P., W.-G. Kim, and Y.-H. Kim, "Large aperture low aberration aspheric dielectric lens antenna for W-band quasi optics," *Progress In Electromagnetics Research*, Vol. 103, 57–65, 2010.
8. Qiu, J., Z. Zhuang, X. Han, and F. Xie, "Design of quasi-optical subsystem for millimeter-wave imaging system," *International Symposium on Antennas Propagation & Em Theory*, 530–533, 2008.
9. Volkov, P. V., Yu. I. Belov, A. V. Goryunov, I. A. Illarionov, et al., "Aspherical single-lens objective for radio-vision systems of the millimeter-wavelength range," *Technical Physics*, Vol. 59, No. 4, 588–593, 2014.
10. Richter, J., A. Hofmann, and L. P. Schmidt, "Dielectric wide angle lenses for millimeter-wave focal plane imaging," *European Microwave Conference*, 1–4, 2001.
11. Goldsmith, P. F., "Quasi-optical techniques," *Proceedings of the IEEE*, Vol. 80, No. 11, 1729–1747, 1992.
12. Goldsmith, P. F., *Quasi Optical Systems: Gaussian Beam Quasi Optical Propagation and Applications*, 130–133, IEEE Press/Chapman & Hall Publishers, Piscataway, 1998.
13. Zhang, Y., J. Wang, Z. Zhao, and J. Yang, "Numerical analysis of dielectric lens antennas using a ray-tracing method and HFSS software," *IEEE Antennas & Propagation Magazine*, Vol. 50, No. 4, 94–101, 2008.
14. Kim, W.-G., N.-W. Moon, J. Kang, and Y.-H. Kim, "Loss Measuring of large aperture quasi-optics for W-band imaging radiometer system," *Progress In Electromagnetics Research*, Vol. 125, 295–309, 2012.
15. Lee, S.-W., M. S. Sheshadri, V. Jamnejad, and R. Mittra, "Refraction at a curved dielectric interface: geometrical optics solution," *IEEE Transactions on Microwave Theory and Techniques*, Vol. 82, No. 1, 12–19, 1982.